Distorted-wave ionization and x-ray production cross sections of the *K* shell of Cu and the *L* shells of Ag, In, and Sn by positron impact

Michael Dingfelder[*]

Department of Physics, East Carolina University, Greenville, North Carolina 27858, USA

Silvina Segui[†]

Centro Atómico Bariloche, Comisión Nacional de Energía Atómica, 8400 San Carlos de Bariloche, Río Negro, Argentina

José M. Fernández-Varea

Facultat de Física, ECM, Universitat de Barcelona, Diagonal 647, E-08028 Barcelona, Spain

We study the ionization cross sections of the *K* shell of Cu and the *L* shells of Ag, In, and Sn by positron impact using the distorted-wave Born approximation, focusing on the near-threshold energy range (below 40 keV) to compare with recent measurements. The distorted-wave formalism proves to be an appropriate approach, especially to describe the shape of the cross-section curves for positrons accurately. Furthermore, we calculate x-ray production cross sections of the considered *L* shells having recourse to two sets of atomic relaxation parameters involved in the conversion from ionization to x-ray production cross sections. The 5%–10% differences in the theoretical values calculated with these parameter sets are apparently not large enough to explain the discrepancy between the distorted-wave curves and the experimental data, particularly for Ag. Other sources of uncertainty that could be affecting these comparisons are discussed.

I. INTRODUCTION

Recently, inner-shell ionization by low-energy positrons has been studied by Nagashima *et al.* [1,2] for the *K* shell of Cu and the *L* shells of Ag, In, and Sn through the detection of characteristic x-ray intensities from thin targets of these elements. The measurements were carried out with their newly developed Si(Li) detector, which enables the acquisition of x-ray spectra with a low background of scattered annihilation photons; this feature is essential in the energy range below 30 keV because otherwise a high background would lead to unacceptably large uncertainties in the experimentally determined cross sections. Their study was partly motivated by an earlier work of Tang *et al.* [3], who reported appreciable discrepancies for x-ray production cross sections by electron impact between experimental results and theoretical calculations done within the framework of the binary-encounter approximation [4] and the plane-wave Born approximation (PWBA) [5]. The ionization processes induced by electrons or positrons differ in the sign of the Coulomb interaction and the absence of exchange effects in the latter case. Both effects are more pronounced at lower energies, close to the ionization threshold. Thus, it was speculated whether ionization by positrons could shed more light on these collision processes and help to understand the observed discrepancies. However, Nagashima *et al.* [1,2] found somewhat similar disagreement between their measured inner-shell ionization cross sections for positron impact and theoretical estimates based on the binary-encounter formalism [6] and the PWBA

with semiempirical Coulomb and relativistic corrections [7]. Specifically, the experimental values for the *L* shells of Ag, In, and Sn are systematically lower than the predictions of these theoretical models. Moreover, the lack of agreement persisted when x-ray production cross sections were compared instead of the ionization cross sections [8]. Only for the Cu *K* shell could the corrected PWBA reproduce the measurements satisfactorily. Nagashima *et al.* suggested that the aforementioned theoretical approaches are inadequate for *L*-shell ionization, a limitation they related to the decreasing threshold energy and increasing target atomic number [8].

From the theoretical point of view, a more sophisticated description of ionizing collisions is achieved by resorting to the distorted-wave Born approximation (DWBA). In this *ab initio* approach the effect of the target atom on the incident projectile is included in a consistent way, which makes the formalism valid for lower energies, particularly near the ionization threshold. In an earlier work [9], the DWBA was employed to compute cross sections for the ionization by electrons of the *K* and *L* shells of several elements, obtaining very good agreement with the previously presented experimental data, a conclusion that is reinforced by more recent measurements and DWBA calculations [10,11]. Equivalent calculations carried out later on by Colgan *et al.* [12,13] are in excellent accordance with that implementation of the DWBA. Furthermore, the DWBA code has been employed successfully to evaluate $L\alpha_{1,2}$ [10,11,14] and $L\beta_1$ [11] x-ray production cross sections by electron impact for various elements.

In Ref. [9] only a couple of comparisons between DWBA ionization cross sections by the impact of positrons and absolute experimental data were included, namely for the *K* shell of Ag and the L_3 subshell of Au [15]. The agreement was found to be satisfactory. However, the severe scarcity of

---

*[*]dingfelderm@ecu.edu

[†]Also at Consejo Nacional de Investigaciones Científicas y Técnicas (CONICET), Argentina.

experimental cross sections for the ionization of atomic inner shells by positrons has precluded so far a thorough assessment of the capability of the DWBA to accurately model such collisions, a task which thus remains to be undertaken.

The present work is, in this context, a modest step toward a more complete evaluation of the DWBA as a suitable theoretical framework to predict accurate cross sections for inner-shell ionization by positron bombardment. To this end, we calculate cross sections for the ionization by positrons of the K shell of Cu ($Z=29$) and the L shells of Ag, In, and Sn ($Z=47$, 49, and 50, respectively), using the DWBA as described in Ref. [9], and compare the theoretical values with the measurements of Nagashima and co-workers [1,2,8]. In the case of L shells, we also determine the corresponding x-ray production cross sections. The influence of the atomic relaxation parameters involved in the conversion from ionization to x-ray production cross sections (fluorescence yields, Coster-Kronig coefficients, emission rates, etc.) is examined by considering two distinct sets of parameters taken from the literature. To compare with additional experimental data [3,16], we calculate electron-impact x-ray production cross sections for the L lines of Ag, In, and Sn utilizing the same DWBA and parameter sets as for positron impact.

The paper is structured as follows. In Sec. II we summarize the theoretical framework adopted to compute ionization cross sections, and exhibit the results obtained for the inner shells of the aforementioned elements. The conversion from ionization to x-ray production cross sections is described in Sec. III A, with a careful selection of two sets of relaxation parameters proposed by different authors. We present and discuss the results obtained for positron and electron impact in Secs. III B and III C, respectively. Finally, some concluding remarks are given in Sec. IV.

II. IONIZATION CROSS SECTIONS

We employ a semirelativistic DWBA to calculate the ionization cross sections of atomic inner shells by electron or positron impact. In this approach, atomic wave functions are described within the independent-electron approximation; only a single (active) atomic electron is involved in the ionization process. One-electron orbitals are obtained from the Dirac equation using self-consistent Dirac-Fock-Slater (DFS) potentials. The projectile (electron or positron) is described employing plane waves which are distorted by the atomic potential (i.e., distorted plane waves). Only the longitudinal part of the interaction between the projectile and the active electron is considered, because the transverse interaction may be disregarded at the relatively low energies addressed in this study. A more detailed account of the formalism and numerical methods can be found in Ref. [9].

For the sake of completeness, we have also performed *ab initio* calculations within the semirelativistic PWBA. The PWBA constitutes a considerable simplification of the DWBA because the initial and final states of the projectile are represented by plane waves instead of distorted waves. This amounts to the complete neglect of Coulomb effects, so that PWBA ionization cross sections become less accurate than their DWBA counterpart near the threshold energy of

TABLE I. DFS binding energies (in keV) of the K shell and L_i subshells of the investigated elements.

Element (Z)	$K(1s_{1/2})$	$L_1(2s_{1/2})$	$L_2(2p_{1/2})$	$L_3(2p_{3/2})$
Cu (29)	8.950			
Ag (47)	25.462	3.781	3.526	3.348
In (49)	27.921	4.214	3.943	3.728
Sn (50)	29.184	4.440	4.161	3.926

the active shell, though it can be improved by introducing semiempirical Coulomb corrections [7,17]. The numerical evaluation of cross sections within the PWBA is outlined in Ref. [18].

Ionization cross sections are computed for incident energies ranging from the binding energy ϵ_b of the considered atomic inner shells up to 4–8 times ϵ_b ($\approx 30-40$ keV). The binding energies are obtained from the self-consistent DFS potentials, and are listed in Table I for the studied shells. These values are in reasonably good agreement with the theoretical binding energies calculated by Deslattes *et al.* [19] within a relativistic many-body framework, and are sufficiently accurate for the present purposes.

The K-shell ionization cross section for positron impact on Cu is shown in Fig. 1. The theoretical DWBA cross section is in excellent accordance with the experimental data from Nagashima *et al.* [1]. For comparison purposes, we have included the prediction of the naked PWBA, i.e., without any Coulomb correction. It can be seen that the PWBA cross section is too large, highlighting the increasing importance of Coulomb effects when the positron energy approaches the ionization threshold. Only at energies much larger than ϵ_b does the PWBA yield reliable results. A simple, semiempirical Coulomb correction to the PWBA was proposed by Hippler [7,17,20], who implemented it in a semianalytical model where the ionization of the active inner shell is described through its (nonrelativistic) hydrogenic generalized oscillator strength. This corrected PWBA is computationally inexpensive and gives realistic cross sections for
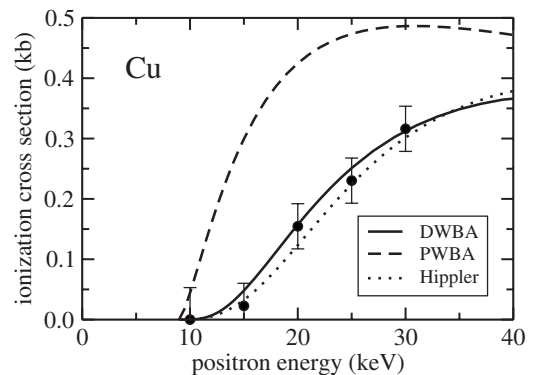

FIG. 1. Cross sections for the ionization of the K shell of Cu by positrons. The solid and dashed curves are the predictions of the DWBA and the PWBA, respectively, whereas the dotted curve indicates Hippler's PWBA with semiempirical relativistic and Coulomb corrections [7,17,20]. The symbols correspond to experimental data from Nagashima *et al.* [1].
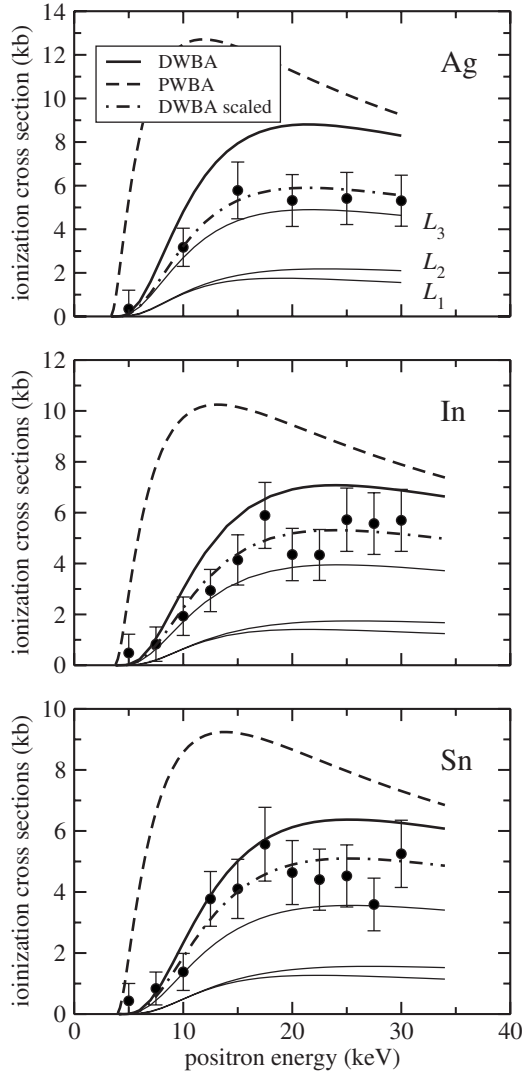
FIG. 2. Cross sections for the ionization of the L shells of Ag, In, and Sn by positrons. The solid and dashed curves are the predictions of the DWBA and the PWBA, respectively. Partial DWBA cross sections for the L_1, L_2, and L_3 subshells are depicted as thin solid curves. The symbols correspond to experimental data from Nagashima *et al.* [1,2]. Scaled DWBA cross sections, i.e., the DWBA values multiplied by a constant factor equal to 0.67, 0.75, and 0.80 for Ag, In, and Sn, respectively, are represented as dotted-dashed curves.

the K shell of atoms with low or intermediate Z, for instance, Cu (see Fig. 1). Unfortunately, Hippler's model is expected to provide less accurate results for L and higher shells due to the progressive inability of hydrogenic wave functions to properly quantify the screening of the nuclear charge by the innermost electrons.

Figure 2 displays L-shell ionization cross sections for positron impact on Ag, In, and Sn. Here it is assumed that the total L-shell ionization cross section is equal to the sum of the three L-subshell contributions, namely $2s_{1/2}$ (L_1), $2p_{1/2}$ (L_2), and $2p_{3/2}$ (L_3). The total and partial DWBA and uncorrected PWBA cross sections are shown for the three elements. The experimental data by Nagashima *et al.* [1,2] are plotted as well. Unlike in the case of the Cu K shell (see Fig.

1), the present DWBA results for the examined L shells reveal systematic differences, which are largest for Ag. However, the shape of the DWBA curves follows the trend of the measurements quite well, so that agreement becomes satisfactory after renormalizing the DWBA cross sections. Thus, total DWBA cross sections multiplied by 0.67 (Ag), 0.75 (In) and 0.80 (Sn) are included in Fig. 2. On the other hand, the PWBA does not account for the difference between electrons and positrons, and is known to overestimate the experimental data. Moreover, the shape of the PWBA curves does not agree with that of the measured curves, i.e., a renormalization will not yield reasonable accordance between experiment and the scaled PWBA.

III. X-RAY PRODUCTION CROSS SECTIONS

The total ionization cross sections reported in Refs. [1,2] were obtained by measuring the x-ray production cross sections and then converting them into total ionization cross sections. The raw data (x-ray production cross sections) for Cu K, Ag L, In L, and Sn L shells have been recently presented in Ref. [8]. The comparison with the predictions of the binary-encounter formalism [6] and the PWBA with semiempirical Coulomb and relativistic corrections [7] showed similar disagreement as in the case of total ionization cross sections. With intent to understand these discrepancies, we set out to calculate the x-ray production cross section for the L shells of Ag, In, and Sn using our DWBA data and atomic relaxation parameters from the literature.

A. Relationships between ionization and x-ray production cross sections

The total x-ray production cross section for the L shell can be written in terms of the ionization cross section of each involved (sub)shell as follows:

$$\sigma_L^x = \sigma_{L_3}\omega_3 + \sigma_{L_2}(\omega_2 + f_{23}\omega_3) + \sigma_{L_1}[\omega_1 + f_{12}\omega_2 + (f_{13} + f'_{13}$$
$$+ f_{12}f_{23})\omega_3] + \sigma_K\{\eta_{KL_1}\omega_1 + (\eta_{KL_2} + f_{12}\eta_{KL_1})\omega_2$$
$$+ [\eta_{KL_3} + f_{23}\eta_{KL_2} + (f_{13} + f'_{13} + f_{12}f_{23})\eta_{KL_1}]\omega_3\}, \quad (1)$$

where σ_{L_i} and σ_K are the ionization cross sections of (sub)shells L_i and K, respectively, ω_i are the fluorescence yields for the L_i subshells, f_{ij} are the Coster-Kronig probabilities between subshells L_i and L_j, f'_{13} is the intrashell radiative yield for transitions of vacancies from L_1 to L_3 (other intrashell transitions are neglected), and η_{KL_i} are the vacancy-transfer probabilities from the K shell to the L_i subshells. Notice that no specific x-ray emission rates are needed to evaluate the total x-ray production cross sections.

Equation (1) corresponds to the sum of the contributions coming from all of the radiative transitions taking place after a vacancy has been produced in any of the three L_i subshells [21]. Often it is possible to distinguish in the recorded x-ray spectrum the contributions from specific transitions or groups of them, such as the $L\ell$ and $L\eta$ lines or the $L\alpha$, $L\beta$, and $L\gamma$ series. The x-ray production cross sections for these lines and line groups are given by (see, e.g., Refs. [21,22])

TABLE II. Fluorescence yields, ω_i, and Coster-Kronig coefficients, f_{ij}, from Krause [23] (set A) and Campbell [24] (set B).

	Krause (set A)			Campbell (set B)		
	Ag	In	Sn	Ag	In	Sn
ω_1	0.016	0.020	0.037	0.0111	0.0134	0.0356
ω_2	0.051	0.061	0.065	0.054	0.064	0.068
ω_3	0.052	0.060	0.064	0.056	0.065	0.070
f_{12}	0.100	0.100	0.170	0.068	0.074	0.188
f_{13}	0.590	0.590	0.270	0.740	0.728	0.323
f_{23}	0.153	0.157	0.157	0.156	0.161	0.167

$$\sigma_{L\ell}^x = \frac{\Gamma_{3\ell}}{\Gamma_{3,\text{total}}}\chi_3, \tag{2}$$

$$\sigma_{L\eta}^x = \frac{\Gamma_{2\eta}}{\Gamma_{2,\text{total}}}\chi_2, \tag{3}$$

$$\sigma_{L\alpha}^x = \frac{\Gamma_{3\alpha}}{\Gamma_{3,\text{total}}}\chi_3, \tag{4}$$

$$\sigma_{L\beta}^x = \frac{\Gamma_{3\beta}}{\Gamma_{3,\text{total}}}\chi_3 + \frac{\Gamma_{2\beta}}{\Gamma_{2,\text{total}}}\chi_2 + \frac{\Gamma_{1\beta}}{\Gamma_{1,\text{total}}}\chi_1, \tag{5}$$

$$\sigma_{L\gamma}^x = \frac{\Gamma_{2\gamma}}{\Gamma_{2,\text{total}}}\chi_2 + \frac{\Gamma_{1\gamma}}{\Gamma_{1,\text{total}}}\chi_1, \tag{6}$$

where $\Gamma_{i\ell}$, $\Gamma_{i\eta}$, $\Gamma_{i\alpha}$, $\Gamma_{i\beta}$, and $\Gamma_{i\gamma}$ are the x-ray emission rates for transitions pertaining to the $L\ell$, $L\eta$, $L\alpha$, $L\beta$, and $L\gamma$ lines or series, and $\Gamma_{i,\text{total}}$ are the emission rates for all possible transitions to the L_i subshell. In the above expressions, the following shorthand notation was adopted [22] (see also Ref. [21]):

$$\chi_1 \equiv \omega_1[\sigma_{L_1} + \eta_{KL_1}\sigma_K], \tag{7}$$

$$\chi_2 \equiv \omega_2[\sigma_{L_2} + f_{12}\sigma_{L_1} + (\eta_{KL_2} + f_{12}\eta_{KL_1})\sigma_K], \tag{8}$$

$$\chi_3 \equiv \omega_3\{\sigma_{L_3} + f_{23}\sigma_{L_2} + (f_{13} + f'_{13} + f_{12}f_{23})\sigma_{L_1} + [\eta_{KL_3} + f_{23}\eta_{KL_2} + (f_{13} + f'_{13} + f_{12}f_{23})\eta_{KL_1}]\sigma_K\}. \tag{9}$$

It is well known from extensive reviews [23,24] that numerical values of the atomic relaxation parameters may present considerable dispersion, even up to ~30%, which could strongly affect the accuracy of the calculated x-ray production cross sections. It is beyond the scope of this work to provide an exhaustive comparison of the various sources of data. Nevertheless, we have chosen two well-differentiated parameter sets from the literature as a simple means to quantify how much the selection of relaxation data may affect the evaluated x-ray production cross sections. A similar (albeit more elaborate) strategy was employed by Miranda *et al.* [25] to examine the influence of atomic relaxation databases

on the production of characteristic x rays by proton bombardment.

Set A is experimentally oriented, with fluorescence yields and Coster-Kronig probabilities taken from the classical compilation of Krause [23]. In turn, set B consists of purely theoretical estimates of ω_i and f_{ij} as reported by Campbell [24]; this author recommends values given by Puri *et al.* [26], which are based on first-principles calculations with relativistic Hartree-Fock-Slater potentials. The two parameter sets for ω_i and f_{ij} adopted in the present analysis are listed in Table II.

The determination of x-ray production cross sections through Eqs. (2)–(6) requires knowledge of the emission rates pertaining to the various series. These are taken from the theoretical work of Scofield [27] for set A, and from the tabulation by Campbell and Wang [28] for set B. The former are based on a Dirac-Hartree-Slater, one-potential, multipole calculation, whereas the latter were obtained by a fit to the Dirac-Fock, two-potential, dipole values also computed by Scofield [29]. Although the two-potential emission rates are presumably more accurate, the older one-potential data are still widely used. Since both tabulations [27,28] list emission rates for single transitions from (sub)shell X_i to Y_j without specifying the series they belong to, we group the transitions for the investigated series as indicated in Table III (if the emission rates are available) using the notation and informa-

TABLE III. Single transitions considered in the L series (as given by Shima *et al.* [30] and Bearden [31]), designated with both the conventional (Siegbahn) and IUPAC notations [32].

Line or group	Transitions
$\Gamma_{3\ell}$	$L\ell$ (L_3M_1)
$\Gamma_{2\eta}$	$L\eta$ (L_2M_1)
$\Gamma_{3\alpha}$	$L\alpha_{2,1}$ ($L_3M_{4,5}$)
$\Gamma_{3\beta}$	$L\beta_6$ (L_3N_1), $L\beta_{15,2}$ ($L_3N_{4,5}$), $L\beta_7$ (L_3O_1)
$\Gamma_{2\beta}$	$L\beta_1$ (L_2M_4)
$\Gamma_{1\beta}$	$L\beta_{4,3}$ ($L_1M_{2,3}$)
$\Gamma_{2\gamma}$	$L\gamma_{5,1}$ ($L_2N_{1,4}$), $L\gamma_8$ (L_2O_1)
$\Gamma_{1\gamma}$	$L\gamma_{2,3}$ ($L_1N_{2,3}$), $L\gamma'_4$ (L_1O_2)
$\Gamma_{i,\text{total}}$	All transitions from the M, N, and O shells to the L_i subshell

TABLE IV. Ratios of emission rates, $\Gamma_{i,\text{series}}/\Gamma_{i,\text{total}}$, from Scofield [27] (set A) and Campbell and Wang [28] (set B).

	Scofield (set A)			Campbell and Wang (set B)		
	Ag	In	Sn	Ag	In	Sn
$\Gamma_{3\ell}/\Gamma_{3,\text{total}}$	0.0329	0.0323	0.0321	0.0324	0.0320	0.0318
$\Gamma_{2\eta}/\Gamma_{2,\text{total}}$	0.0261	0.0253	0.0249	0.0261	0.0253	0.0249
$\Gamma_{3\alpha}/\Gamma_{3,\text{total}}$	0.8801	0.8652	0.8582	0.8701	0.8551	0.8487
$\Gamma_{3\beta}/\Gamma_{3,\text{total}}$	0.0869	0.1022	0.1088	0.0975	0.1129	0.1195
$\Gamma_{2\beta}/\Gamma_{2,\text{total}}$	0.8851	0.8707	0.8645	0.8757	0.8610	0.8546
$\Gamma_{1\beta}/\Gamma_{1,\text{total}}$	0.8414	0.8312	0.8255	0.8352	0.8262	0.8224
$\Gamma_{2\gamma}/\Gamma_{2,\text{total}}$	0.0879	0.1033	0.1101	0.0982	0.1137	0.1204
$\Gamma_{1\gamma}/\Gamma_{1,\text{total}}$	0.1497	0.1588	0.1646	0.1568	0.1657	0.1755

tion provided by Shima *et al.* [30] and Bearden [31], respectively. Notice that only dipole-allowed transitions are included. The corresponding $\Gamma_{i,\text{series}}/\Gamma_{i,\text{total}}$ ratios are displayed in Table IV for the two data sets.

Finally, vacancy-transfer probabilities η_{KL_i} are taken from Rao *et al.* [33] for both parameter data sets. They are based on semiempirical estimates, and include radiative (R) and Auger (A) contributions, i.e., $\eta_{KL_i} = \eta_{KL_i}(R) + \eta_{KL_i}(A)$; recall that $\eta_{KL_1}(R) = 0$ in the dipole approximation. Rao *et al.* provide this information only for even values of Z; since this curve is smooth, linear interpolation was applied to obtain the vacancy-transfer probabilities for Ag and In. The sums $\Sigma_{i=1}^{3} \eta_{KL_i}$ are in good agreement with existing measurements [34]. In addition, the intrashell radiative yields f'_{13} are taken from Krause [23] in the two parameter sets. All values used in the calculations are listed in Table V. It should be borne in mind that the actual selection of η_{KL_i} and f'_{13} will have a minor influence on the evaluation of x-ray production cross sections because the corresponding terms are much smaller than the others; nevertheless, for the sake of completeness they are kept in the present analysis.

B. Results for positron impact

The total L shell x-ray production cross sections and the contributions of lines or series $L\ell$, $L\eta$, $L\alpha$, $L\beta$, and $L\gamma$ were calculated from the DWBA ionization cross sections by positron impact presented in Sec. II, using the selected values (sets A and B) for the atomic relaxation parameters. Figure 3 displays the results obtained for Ag, In, and Sn with both

TABLE V. Yields for the transition of vacancies from the K shell to the L_i subshells, η_{KL_i}, as given by Rao *et al.* [33]. Values for intrashell radiative yield, f'_{13}, are from Krause [23].

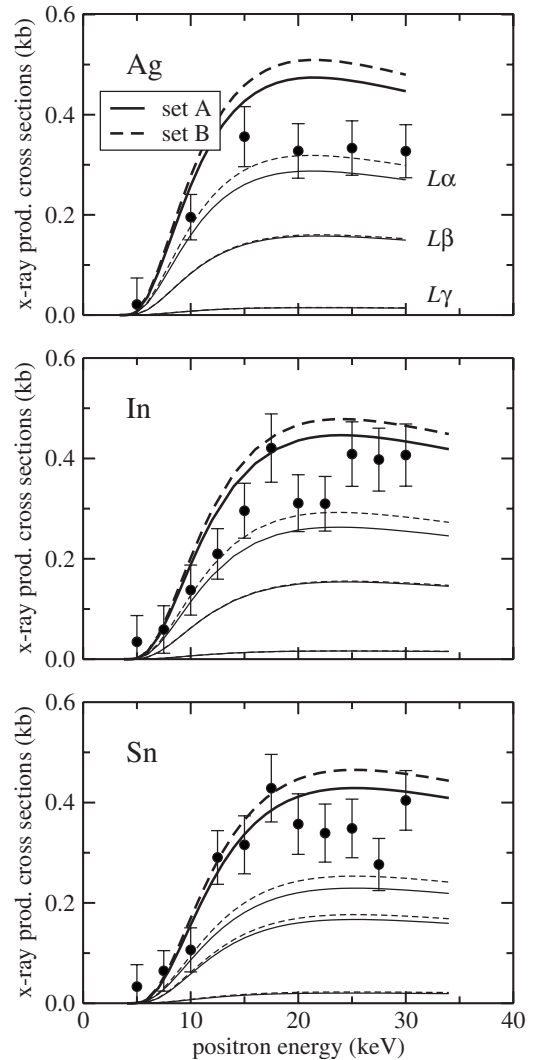|	η_{KL_1}	η_{KL_2}	η_{KL_3}	f'_{13}
Ag	0.0688	0.3211	0.5725	1.2×10^{-4}
In	0.0621	0.3145	0.5655	1.6×10^{-4}
Sn	0.0588	0.3114	0.5620	3.0×10^{-4}

FIG. 3. Total L-lines x-ray production cross sections of Ag, In, and Sn by positrons, calculated with Eq. (1). The solid and dashed curves are present results computed with the DWBA and parameter sets A and B, respectively. The symbols correspond to experimental data from Nagashima *et al.* [8]. X-ray production cross sections for the $L\alpha$, $L\beta$, and $L\gamma$ series obtained with sets A and B are represented as thin solid and dashed curves, respectively.

parameter data sets A and B in order to assess their influence on the accuracy of the evaluated partial and total x-ray production cross sections. The contributions of lines $L\ell$ and $L\eta$ are not shown as these curves would clutter the figure. Besides, the experimental data from Ref. [8] are plotted with their associated uncertainties. As in the case of the ionization cross sections, the form of the curves obtained for total x-ray production cross sections is very well reproduced by the DWBA, but the experimental points lie between the $L\alpha$ and the total L curves. Cross sections evaluated with set A are somewhat closer to the measurements. Although the differences between the x-ray production cross sections obtained by using either data set A or B can be significant, up to around 5%–10%, they are smaller than the apparent systematic deviation of the DWBA curves (absolute values) relative to the measured data, especially for Ag.

The systematically lower experimental x-ray production cross sections might be partly due to incomplete collection of characteristic x rays. For elements with $Z \sim 50$ and typical resolutions around 150–200 eV full width at half-maximum (FWHM) at the Mn $K\alpha$ line (5.9 keV) of energy-dispersive spectrometers [3,16,22,35], there is a certain overlap between the $L\alpha$ and $L\beta$ peaks [see, e.g., Fig. 1(c) in Ref. [35]]. The resolution of the thin Si(Li) detector developed by Nagashima *et al.* [1,2] is 300 eV at 5.9 keV, which makes the $L\alpha$ and $L\beta$ lines appear as a single, broad peak [see Fig. 1(b) in Ref. [1]]. Nonetheless, lines $L\ell$ and, to some extent, also $L\eta$ and $L\gamma$, may in principle be resolved from the $L\alpha+L\beta$ peak. However, the large fluctuations of the background in the spectra acquired by Nagashima and co-workers could easily mask these weaker lines, whose emission rates are about 0.03. Then, if characteristic x rays corresponding to these lines are "lost" when the background is subtracted, the experimentally determined x-ray production cross section would be $\sim 5\%$–10% lower. Although transition $L\gamma_5$ is closer to $L\beta$ than to $L\gamma_{2,3}$ and may overlap with the $L\alpha+L\beta$ peak, our reasoning might still account for part of the reduction. Furthermore, a tentative explanation for the diminishing differences between theory and experiment with Z (when passing from Ag to In and Sn the rescaling factor that brings the DWBA into agreement with the measurements becomes closer to 1) is the following. The energies of the L peaks increase with Z, moving them away from the region where the background due to positron annihilation is largest (it grows for decreasing energies), and therefore making background subtraction a less delicate issue. New measurements for elements with atomic numbers slightly above 50 would be valuable to confirm or rule out these explanations. On the other hand, even if differences between x-ray production cross sections calculated with sets A and B do not exceed $\sim 10\%$, the possibility of larger uncertainties in some of the relaxation parameters cannot be excluded and could certainly account for the remaining part of the disagreement.

A similar comparison of theoretical (DWBA and PWBA) $L\alpha_{1,2}$ and $L\beta_1$ x-ray production cross sections and experiment was recently conducted by Merlet *et al.* [11] for the L shells of Ga and As and electron impact. They found that the shape of the DWBA was in good agreement with measurements, and the deviations in the absolute values were ascribed to the uncertainties in the relaxation parameters. This
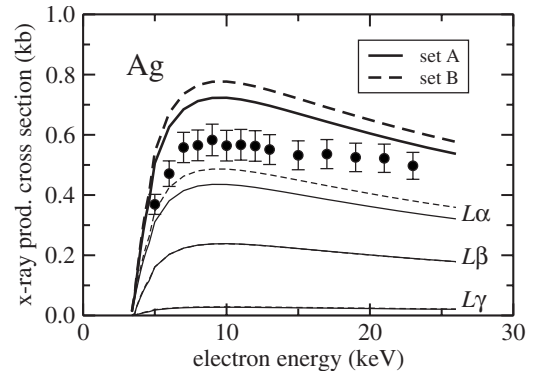

FIG. 4. Total L-lines x-ray production cross sections of Ag by electrons, calculated with Eq. (1). The solid and dashed curves are present results computed with the DWBA and parameter sets A and B, respectively. The symbols correspond to experimental data from Wu *et al.* [16]. X-ray production cross sections for the $L\alpha$, $L\beta$, and $L\gamma$ series obtained with sets A and B are represented as thin solid and dashed curves, respectively.

conclusion is plausible (and does not conflict with our previous argument) due to the high resolution of their wavelength-dispersive spectrometer, which enabled the clear separation of the measured $L\alpha_{1,2}$ and $L\beta_1$ peaks from neighboring ones, and the low background of the recorded spectra.

C. Results for electron impact

To put the previous findings in perspective, x-ray production cross sections were calculated for the L shells of Ag, In, and Sn by electron bombardment with the same DWBA formalism and relaxation parameters as in the case of positrons. Available measurements to compare with are from Wu *et al.* [16] (Ag) and Tang *et al.* [3] (In and Sn). These experiments were carried out on thin samples deposited on thick Al substrates, so that the raw x-ray spectra had to be corrected for the perturbation introduced by the substrates; this was done either having recourse to Monte Carlo simulation [16] or through analytical methods [3]. Total x-ray production cross sections for Ag are presented in Fig. 4. The theoretical curve evaluated with set A is again in slightly better agreement with the measurements. On the other hand, the experimental setup of Tang and co-workers (in particular the energy resolution of 170 eV FWHM at 5.9 keV) permitted the separation of the $L\alpha$ and $L\beta$ peaks, and comparison of the DWBA cross sections with their data is therefore of a higher significance. Results are depicted in Fig. 5, left-hand column. The overall agreement between theory and experiment is quite satisfactory. Set B yields $L\alpha$ x-ray production cross sections that are in somewhat better accord with the measurements than values obtained using set A. As shown in Fig. 5, right-hand column, the experimental $L\beta/L\alpha$ ratios are nearly constant for energies above around 1.5 times the binding energy, and the theoretical predictions closely match those values. For Sn, the $L\beta/L\alpha$ and $L\gamma/L\alpha$ ratios measured by Baxter and Spicer at 20 keV [21] practically coincide with our data evaluated using set A. It is worth stressing that quotients of x-ray production cross sections have smaller uncertainties
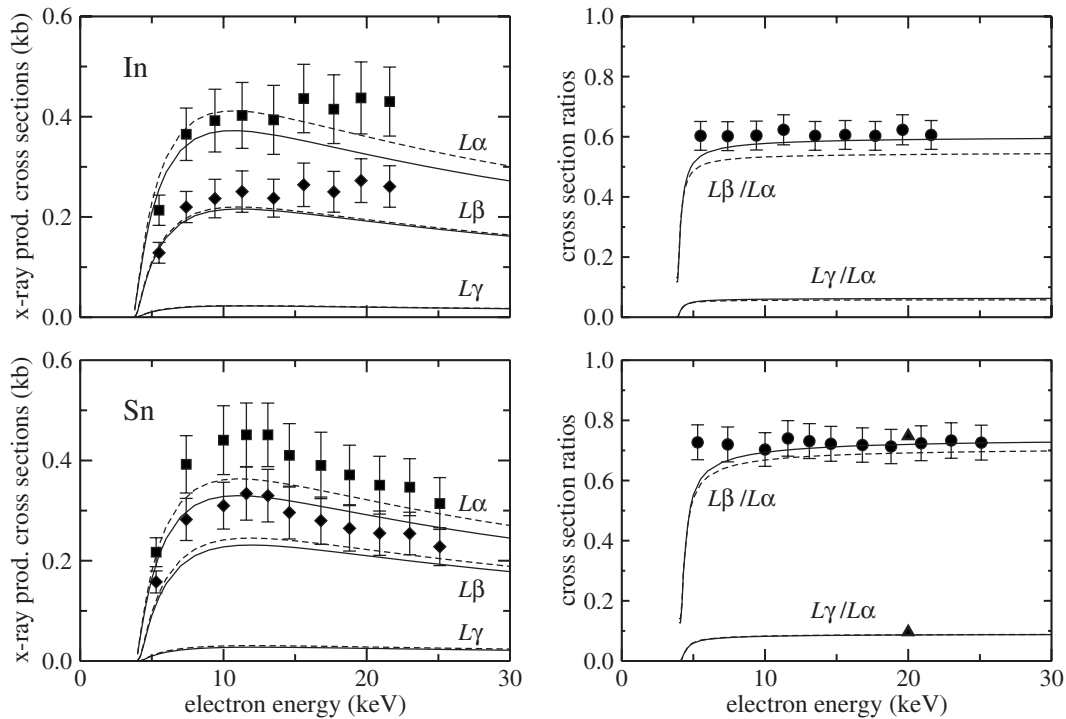
FIG. 5. X-ray production cross sections of In and Sn by electrons, calculated using the DWBA formalism and either parameter set A (solid curves) or B (dashed curves). Left-hand graphs: Cross sections for the production of $L\alpha$, $L\beta$, and $L\gamma$ x rays. Symbols are experimental data for $L\alpha$ and $L\beta$ from Tang *et al.* [3]. Right-hand graphs: $L\beta/L\alpha$ and $L\gamma/L\alpha$ ratios of cross sections. Symbols are experimental data from Tang *et al.* [3] (circles) and Baxter and Spicer [21] (triangles).

than the cross sections themselves. This is because the areas of the x-ray peaks in the experimental spectrum are proportional to the thickness of the irradiated sample and the detector efficiency (which varies slowly with photon energy). These two quantities cancel out when ratios are reported, and consequently their uncertainties (far from negligible in the case of the thickness) do not contribute to that of the ratio. All these results reinforce the expectation that the DWBA is a reliable model to predict accurate ionization (and hence x-ray production) cross sections of atomic inner shells.

IV. CONCLUSIONS

We have employed the semirelativistic DWBA to calculate ionization cross sections of the K shell of Cu and the L shells of Ag, In, and Sn by positron impact. The absolute DWBA values for the Cu K shell are in superb agreement with the experimental data of Nagashima *et al.* [1]. On the other hand, in the case of the L shells the predictions of the DWBA are larger than the measurements reported by them [1,2], but the shape of the DWBA cross sections is in good accord with those measurements. In this respect, the DWBA is superior to simpler models like the binary-encounter approximation [6] or the (uncorrected) PWBA.

In order to ascertain the cause of the observed discrepancies, we computed the corresponding x-ray production cross sections from the DWBA ionization cross sections so as to compare with the raw experimental data from Nagashima *et al.* [8]. Two sets of atomic relaxation parameters were

chosen, one based on an experimental compilation and the other on theoretical values. The x-ray production cross sections obtained with the two data sets differ less than around 10%, seemingly not enough to explain the systematic deviation of the absolute values. The difficulty to discern experimentally the weak $L\ell$ and $L\gamma$ peaks from the fluctuations of the background may partially account for the lower experimental cross sections, especially for Ag.

To complete our analysis, we have calculated total and $L\alpha$, $L\beta$, and $L\gamma$ x-ray production cross sections for electron impact on Ag, In, and Sn using the same DWBA formalism and relaxation data. The theoretical values are in fair agreement with the total x-ray production cross sections for Ag measured by Wu *et al.* [16], while the agreement with the $L\alpha$ and $L\beta$ cross sections of In and Sn reported by Tang *et al.* [3] is encouraging. In turn, the calculated $L\beta/L\alpha$ and $L\gamma/L\alpha$ ratios coincide with the experimental ones from the latter work and from Ref. [21].

In summary, for the studied elements and inner shells the DWBA is found to provide ionization and x-ray production cross sections that compare rather well with measurements. Experiments are difficult owing to, among other things, the limited energy resolution of existing spectrometers or the distortion of the recorded signal when the samples are deposited on thick substrates. The situation is further complicated in the case of positrons due to the high background originated from annihilation photons. The ensuing shortage of experimental cross sections for the ionization of atomic inner shells by positrons impedes at present a comprehensive assessment of the DWBA for these projectiles.

A shortcoming of the presently used implementation of the DWBA [9] is that convergence problems limit its applicability to the interval from the binding energy ϵ_b of the active shell up to 8–10 times ϵ_b. When the projectile energy exceeds about 20 times ϵ_b the PWBA yields accurate ionization cross sections. A fully relativistic PWBA has been formulated very recently by Bote and Salvat [36], who also obtained distortion and exchange corrections to the PWBA, thus enabling theoretical calculations to be carried out up to arbitrarily high energies.

[1] Y. Nagashima, F. Saito, Y. Itoh, A. Goto, and T. Hyodo, Phys. Rev. Lett. **92**, 223201 (2004); **92**, 239902(E) (2004).

[2] Y. Nagashima, W. Shigeta, T. Hyodo, F. Saito, Y. Itoh, A. Goto, and M. Iwaki, in *Proceedings of the XXIV International Conference on Photonic, Electronic and Atomic Collisions (ICPEAC), Rosario, Argentina, 2005*, edited by P. D. Fainstein, M. A. P. Lima, J. E. Miraglia, E. C. Montenegro, and R. D. Rivarola (World Scientific, Singapore, 2006), pp. 399–406.

[3] C. Tang, Z. Luo, Z. An, F. He, X. Peng, and X. Long, Phys. Rev. A **65**, 052707 (2002).

[4] M. Gryziński, Phys. Rev. **138**, A336 (1965).

[5] E. J. McGuire, Phys. Rev. A **16**, 73 (1977).

[6] M. Gryziński and M. Kowalski, Phys. Lett. A **183**, 196 (1993).

[7] S. P. Khare and J. M. Wadehra, Can. J. Phys. **74**, 376 (1996).

[8] Y. Nagashima, W. Shigeta, T. Hyodo, and M. Iwaki, Radiat. Phys. Chem. **76**, 465 (2007).

[9] S. Segui, M. Dingfelder, and F. Salvat, Phys. Rev. A **67**, 062710 (2003).

[10] C. Merlet, X. Llovet, and F. Salvat, Phys. Rev. A **69**, 032708 (2004).

[11] C. Merlet, X. Llovet, and J. M. Fernández-Varea, Phys. Rev. A **73**, 062719 (2006); **74**, 049901(E) (2006).

[12] J. Colgan, C. J. Fontes, and H. L. Zhang, Phys. Rev. A **73**, 062711 (2006).

[13] J. Colgan (private communication).

[14] C. S. Campos, M. A. Z. Vasconcellos, X. Llovet, and F. Salvat, Phys. Rev. A **66**, 012719 (2002).

[15] H. Schneider, I. Tobehn, F. Ebel, and R. Hippler, Phys. Rev. Lett. **71**, 2707 (1993).

[16] Y. Wu, Z. An, M. T. Liu, Y. M. Duan, C. H. Tang, and Z. M. Luo, J. Phys. B **37**, 4527 (2004).

[17] R. Hippler, Phys. Lett. A **144**, 81 (1990).

[18] S. Segui, M. Dingfelder, J. M. Fernández-Varea, and F. Salvat, J. Phys. B **35**, 33 (2002).

[19] R. D. Deslattes, E. G. Kessler, Jr., P. Indelicato, L. de Billy, E. Lindroth, and J. Anton, Rev. Mod. Phys. **75**, 35 (2003).

[20] Z. An, Z. M. Luo, and C. Tang, Nucl. Instrum. Methods Phys. Res. B **179**, 334 (2001).

[21] G. W. Baxter and B. M. Spicer, Aust. J. Phys. **36**, 287 (1983).

[22] I. Han, L. Demir, and M. Ağbaba, Radiat. Phys. Chem. **76**, 1551 (2007).

[23] M. O. Krause, J. Phys. Chem. Ref. Data **8**, 307 (1979).

[24] J. L. Campbell, At. Data Nucl. Data Tables **85**, 291 (2003).

[25] J. Miranda, C. Romo-Kröger, and M. Lugo-Licona, Nucl. Instrum. Methods Phys. Res. B **189**, 21 (2002).

[26] S. Puri, D. Mehta, B. Chand, N. Singh, and P. N. Trehan, X-Ray Spectrom. **22**, 358 (1993).

[27] J. H. Scofield, At. Data Nucl. Data Tables **14**, 121 (1974).

[28] J. L. Campbell and J.-X. Wang, At. Data Nucl. Data Tables **43**, 281 (1989).

[29] J. H. Scofield, Phys. Rev. A **10**, 1507 (1974); **12**, 345(E) (1975).

[30] K. Shima, T. Nakagawa, K. Umetani, and T. Mikumo, Phys. Rev. A **24**, 72 (1981).

[31] J. A. Bearden, Rev. Mod. Phys. **39**, 78 (1967).

[32] R. Jenkins, R. Manne, R. Robin, and C. Senemaud, Pure Appl. Chem. **63**, 735 (1991).

[33] P. V. Rao, M. H. Chen, and B. Crasemann, Phys. Rev. A **5**, 997 (1972).

[34] Ö. Şimşek, D. Karagöz, and M. Ertugrul, Spectrochim. Acta, Part B **58**, 1859 (2003).

[35] W. Jitschin, R. Stötzel, T. Papp, and M. Sarkar, Phys. Rev. A **59**, 3408 (1999).

[36] D. Bote and F. Salvat, Phys. Rev. A **77**, 042701 (2008).